PNAS RESEARCH ARTICLE | BIOCHEMISTRY

The SHDRA syndrome-associated gene *TMEM260* encodes a protein-specific O-mannosyltransferase

Ida Signe Bohse Larsen[a,1], Lorenzo Povolo[a,1], Luping Zhou[b], Weihua Tian[a,2], Kasper Johansen Mygind[a,3], John Hintze[a], Chen Jiang[b], Verity Hartill[c,d], Katrina Prescott[d], Colin A. Johnson[c], Sureni V. Mullegama[e], Allyn McConkie-Rosell[f], Marie McDonald[f], Lars Hansen[a], Sergey Y. Vakhrushev[a], Katrine T. Schjoldager[a], Henrik Clausen[a], Thomas Worzfeld[b,g], Hiren J. Joshi[a,4], and Adnan Halim[a,4]

Edited by Robert S. Haltiwanger, The University of Georgia, Athens, GA; received February 14, 2023; accepted April 21, 2023 by Editorial Board Member Stephen J. Benkovic

Mutations in the *TMEM260* gene cause structural heart defects and renal anomalies syndrome, but the function of the encoded protein remains unknown. We previously reported wide occurrence of O-mannose glycans on extracellular immunoglobulin, plexin, transcription factor (IPT) domains found in the hepatocyte growth factor receptor (cMET), macrophage-stimulating protein receptor (RON), and plexin receptors, and further demonstrated that two known protein O-mannosylation systems orchestrated by the POMT1/2 and transmembrane and tetratricopeptide repeat-containing proteins 1-4 gene families were not required for glycosylation of these IPT domains. Here, we report that the *TMEM260* gene encodes an ER-located protein O-mannosyltransferase that selectively glycosylates IPT domains. We demonstrate that disease-causing *TMEM260* mutations impair O-mannosylation of IPT domains and that *TMEM260* knockout in cells results in receptor maturation defects and abnormal growth of 3D cell models. Thus, our study identifies the third protein-specific O-mannosylation pathway in mammals and demonstrates that O-mannosylation of IPT domains serves critical functions during epithelial morphogenesis. Our findings add a new glycosylation pathway and gene to a growing group of congenital disorders of glycosylation.

glycosylation | congenital disorders of glycosylation | O-mannosylation | glycoproteomics | plexin

Significance

We demonstrate that the *TMEM260* gene encodes a novel protein-specific O-mannosyltransferase that selectively glycosylates a common protein domain shared among cMET, RON, and plexin receptors. Biallelic mutations in *TMEM260* underlie structural heart defects and renal anomalies syndrome (SHDRA), a severe developmental disorder associated with congenital cardiac malformations and early childhood mortality. We show that disease-causing mutations impair the TMEM260 O-mannosyltransferase function, which affects proprotein maturation and intracellular trafficking of receptor substrates and epithelial morphogenesis. Our study uncovers a third biosynthetic pathway for protein O-mannosylation in higher eukaryotes and identifies SHDRA as a new congenital disorder of glycosylation.

Congenital disorders of glycosylation (CDGs) are a continuously expanding group of metabolic disorders caused by deficiencies in glycosylation of proteins or lipids (1). More than 50 distinct CDGs are caused by loss of function of glycosyltransferase genes involved in different protein N- and as O-glycosylation pathways (1, 2), and in particular glycosyltransferase genes dedicated to protein O-mannosylation pathways have been identified as causing CDGs (3, 4). The clinical presentation of CDGs often involve multisystemic syndrome features without clear evidence pointing to glycosylation deficiencies, and discovery of novel CDGs often rely on identification of involved genes by whole-exome sequencing (1). It remains challenging to identify genes as glycosylation enzymes. However, new protein O- and C-mannosylation enzymes and novel CDGs have been identified within the last decade (5). Recently, biallelic mutations in the gene *TMEM260* were identified in affected individuals of several consanguineous families characterized by structural heart defects, kidney abnormalities, neurological disorders, and perinatal death in a syndrome designated structural heart defects and renal anomalies syndrome (SHDRA) (OMIM: 617478) (6, 7). The causal role of the *TMEM260* gene was validated in a zebrafish model by gene knockout (KO) and rescue (7), but the function of the encoded protein and molecular basis for effects remained obscure.

We separately identified TMEM260 in a bioinformatic screen for putative multi-pass transmembrane (TM) glycosyltransferases using the Pfam database in course of searching for a novel type of protein O-mannosylation (4). The predicted domain structure of TMEM260 shows similarity to protein O-mannosyltransferases, POMT1 and POMT2 (8), for which deficiencies cause different forms of muscular dystrophy-dystroglycanopathies (9, 10), and the more recently discovered TM and tetratricopeptide repeat-containing proteins 1-4 (TMTC1-4) (11), for which deficiencies in TMTC3 cause brain malformations, e.g. cobblestone lissencephaly (12), and periventricular nodular heterotopia (13), while other TMTCs are associated with hearing loss (14, 15). The protein O-mannosyltransferase 1 and 2 (POMT1/2) and TMTC1-4 are distinct families of protein mannosyltransferase isoenzymes serving different classes of protein clients (4). POMT1/2 transfer O-linked mannose (O-Man) to alpha-dystroglycan (αDG) of the dystrophin-glycoprotein complex (DGC) where elongated complex O-Man glycans on αDG mediate interactions between extracellular matrix proteins, the DGC, and the cellular cytoskeleton (16). The TMTC1-4 family transfer O-Man to the

This article is a PNAS Direct Submission. R.S.H. is a guest editor invited by the Editorial Board.

[1]I.S.B.L. and L.P. contributed equally to this work.

[2]Present address: Section for Protein Science and Biotherapeutics, Department of Biotechnology and Biomedicine, Technical University of Denmark, 2800 Copenhagen, Denmark.

[3]Present address: Biotech Research and Innovation Center, University of Copenhagen, 2200 Copenhagen N, Denmark.

[4]To whom correspondence may be addressed. Email: joshi@sund.ku.dk or halim@sund.ku.dk.

This article contains supporting information online at https://www.pnas.org/lookup/suppl/doi:10.1073/pnas.2302584120/-/DCSupplemental.

Published May 15, 2023.

extracellular cadherin (EC) domains of the cadherin superfamily, including E- and N-cadherin and clustered/non-clustered protocadherins (11, 17, 18). However, we previously identified a third class of O-mannosylated proteins characterized by extracellular immunoglobulin, plexin, transcription factor (IPT) domains, which were not dependent on the functions of the POMT1/2 and TMTC1-4 protein O-mannosyltransferase isoenzymes (4, 11). Thus, identification of TMEM260 as a protein with structural similarity to these mannosyltransferases prompted us here to investigate a putative role of TMEM260 in O-mannosylation of extracellular IPT domains. Using CRISPR/Cas9 genetic engineering and O-Man glycoproteomics, we demonstrate that *TMEM260* encodes an ER-located protein that indeed is selectively required for O-mannosylation of extracellular IPT domains of cMET, RON, and multiple plexin receptors. We describe two novel patient families with *TMEM260* mutations linked to the SHDRA syndrome (6), and demonstrate that these mutations selectively impair glycosylation of IPT domains.

Results

Identification of *TMEM260* as a Candidate O-Mannosyltransferase Gene. We hypothesized that the candidate protein would show structural similarity (Glycosyltransferase superfamily C (GT-C) folds) (19), but not necessarily significant sequence similarity (11) to the POMTs and TMTCs, or the DPY-19 protein C-mannosyltransferases (20), classified in the GT39, GT105, and GT98 families in CAZy, respectively (21). Candidate screening relied on the PMT yeast orthologs of POMTs. Yeast PMTs match the PMT_2 superfamily domain hmm model (cl21590), and specifically the PMT_2 PFAM model (pfam13231). Using the Conserved Domain Architecture Retrieval Tool (22), we identified sequences in early metazoans that matched the PMT_2 model and found a group of proteins that frequently matched with a sequence model for DUF2723. The sequence model was traced in higher organisms and matched with the *TMEM260* gene predicted to encode a 79 kDa multipass TM protein. AlphaFold (23) predicts TMEM260 to share the GT-C fold characteristic for mannosyltransferases, including a conserved N-terminal GT-C module and a variable C-terminal module (Fig. 1) (24, 25). The N-terminal region of TMEM260 adopts the GT-C module (Fig. 1*C*) commonly found among enzymes that utilize lipid-linked donor sugars, including PMT1/PMT2 (26), ALG6 (25), PglB (27), STT3 (28, 29), ArnT (30) and DPY19 (24) glycosyltransferases. The N-terminal (residues 1 to 410) of TMEM260 is predicted to comprise 11 TM helixes of which TM1-TM7 are superimposable (Fig. 1*E*) with the conserved GT-C module of PMT1 (26), while the C-terminal region (residues 411 to 707) partially includes tetratricopeptide (TPR) repeats (31) as found in the TMTC1-4 (GT105) and OGT (GT41) glycosyltransferases (32, 33). The first predicted ER-luminal loop of TMEM260 aligns well with the corresponding loop of PMT1, with Asp52 of TMEM260 closely positioned to and oriented toward the same space as the catalytically important Asp77 of PMT1 (34), which faces the co-purified dolichol-phosphate lipid in the PMT1 structure (Fig. 1*F*), suggesting that Asp52 of TMEM260 may be important for catalytic functions. Like the TMTC1-4 isoenzyme family, the C-terminal region of TMEM260 protrudes into the ER-lumen (*SI Appendix*, Fig. S2), where the predicted TPR domain is likely involved in substrate recognition and selective recruitment of IPT-domains for O-Man glycosylation.

***TMEM260* Encodes a Protein O-Mannosyltransferase Selectively Serving IPT Domains.** Transient expression of tagged TMEM260 (TMEM260-3×FLAG) in BG1 human ovarian cancer cell line (35) indicated ER-localization (Fig. 1*G*), which is in agreement with the presence of di-arginine ER-retention motif at residues 20 to 22 (36) and consistent with the established subcellular localization of POMTs and TMTCs (37–39). We used anti-FLAG purification followed by bottom-up mass spectrometry analyses to demonstrate N-glycosylation at Asn569, which indicated that the most C-terminal region (residues 411 to 707) of TMEM260 faces the ER lumen (*SI Appendix*, Fig. S2). We used CRISPR/Cas9 mediated KO of *TMEM260* in HEK293 SimpleCells (HEK293$^{SC/KO:TMEM260}$), and employed human HEK293^{SC} with KO of *COSMC* and *POMGNT1* that do not elongate O-glycans to enable sensitive enrichment of O-Man glycopeptides by Concanavalin A (ConA) lectin chromatography (11, 18). Mass spectrometry analysis of total cell extracts from HEK293^{SC} and HEK293$^{SC/KO:TMEM260}$ differentially labeled with stable isotopes revealed selective loss of O-Man glycopeptides derived from IPT domains (Fig. 2 and Dataset S1), including plexins (plexin A1-4, B1-2 and D1), hepatocyte growth factor receptor (cMET), and the macrophage-stimulating protein receptor (RON). Notably, KO of *TMEM260* did not influence O-Man glycopeptides derived from αDG and cadherins that are dependent on POMTs and TMTCs, respectively, as previously shown (Fig. 2) (11, 18). This analysis was replicated with cell lysates of HEK293^{WT} and HEK293$^{KO:TMEM260}$ cells (Dataset S1), which corroborated selective loss of O-Man glycopeptides derived from IPT domains in HEK293$^{KO:TMEM260}$. We further reintroduced TMEM260 by site-directed knock-in (KI) in the HEK293$^{KO:TMEM260}$ cells, which resulted in full rescue of O-Man glycopeptides from IPT domains (Fig. 2*D* and Dataset S1). Finally, we speculated that Asp52 of TMEM260 serves important functions based on the structural alignment of D52 with the catalytically important D77 of yeast PMT1 (Fig. 1*F*). To test this hypothesis, we generated a D52A mutant and knocked-in the *TMEM260* D52A variant in HEK293$^{KO:TMEM260}$ cells. Western blot (WB) analyses revealed that expression of *TMEM260* D52A was indistinguishable from *TMEM260* WT upon KI in HEK293$^{KO:TMEM260}$ cells (Fig. 2*C*). In contrast, differential glycoproteomic analyses revealed that TMEM260 D52A was unable to restore O-Man glycosylation on IPT domains (Fig. 2*C*). We also expressed a full-length cMET-3×FLAG fusion protein in HEK293^{WT} and HEK293$^{SC/KO:TMEM260}$ cells and used label-free quantification to demonstrate high O-Man occupancy at Thr582 (68%), Thr676 (100%), and Thr761 (44%) on β-strands in three IPT domains of the mature cMET β-chain (*SI Appendix*, Fig. S3). The O-Man glycans were sensitive to jack bean alpha-mannosidase digestion, confirming α-anomeric configuration of the linkage (Manα1-O-Ser/Thr) (*SI Appendix*, Fig. S3). We utilized the open search Mass spectrometry (MS) Fragger tool (40) for unbiased mining of the MS/MS data and found no evidence of elongated O-Man glycans (*SI Appendix*, Fig. S4), which indicates that the TMEM260-directed O-mannosylation pathway may not undergo elongation. This is similar to the TMTC directed O-mannosylation, while the POMT directed O-mannosylation of α-DG undergo complex modifications (41). Taken together, these results demonstrate that the *TMEM260* gene encodes a protein O-mannosyltransferase that serves a highly select group of protein clients with IPT domains that is distinct from the clients served by the POMTs and TMTCs. The TMEM260 enzyme will therefore be classified as a new distinct GT117 family in the CAZy database (21).

Disease-Causing Mutations in *TMEM260* Affect O-Mannosylation Functions. The SHDRA syndrome caused by mutations in the *TMEM260* gene (6, 7) was predicted to have relative high

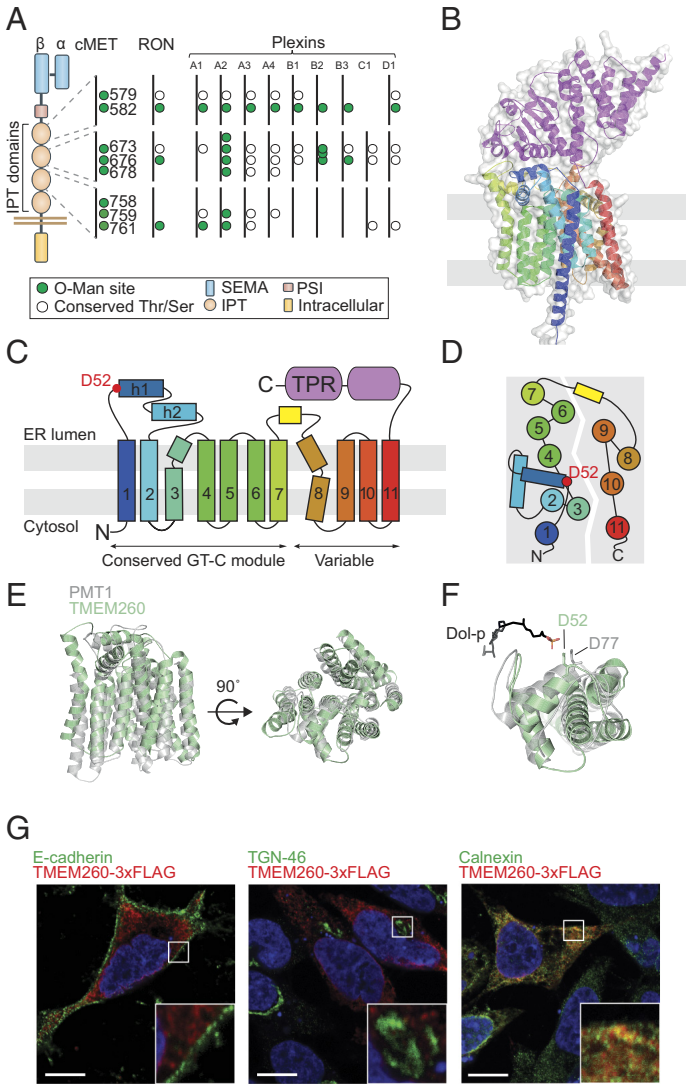

Fig. 1. TMEM260 shares structural similarity with GT-C enzymes. (*A*) Domain organization of cMET, RON and plexin receptors; IPT domains are O-Man glycosylated (green circle) on conserved Ser/Thr residues (hollow circle; not detected with O-Man). (*B*) Alphafold model of TMEM260 showing the N-terminal transmembrane domain (rainbow) and the ER-luminal C-terminal domain (purple). (*C*) Predicted membrane topology and (*D*) position of transmembrane and ER-luminal domains, colored as (*B*). The position of the D52, predicted to be important for TMEM260 functions, is indicated by a red circle. (*E*) Structural alignment of the 7TM conserved GT-C module for PMT1 (gray) and TMEM260 (green). (*F*) Structural alignment of the amino-terminal segment including the first three transmembrane helixes for PMT1 (gray) and TMEM260 (green), demonstrating that D52 of TMEM260 is positioned in the same orientation and space as the critical D77 residue of PMT1. The co-purified lipid-linked donor Dolichol phosphate (Dol-P) of PMT1 is shown in black (dolichol) and red (phosphate). (*G*) BG1 cells transiently expressing TMEM260-3×FLAG fusion protein. Sub-cellular localization of TMEM260 with ER (Calnexin), Golgi (TGN-46) and cell-surface (E-cadherin) markers demonstrate that TMEM260 resides in the ER compartment. (Scale bar: 10 μm.)

carrier frequency in select populations with ranges from 0.0007 to 0.007 across ancestries. To confirm that predicted deleterious mutations affected the O-Man glycosylation function, we analyzed two reported homozygous *TMEM260* mutations, c.1393C>T; p.Q465* and c.1698_1701del; p.Y567Tfs*27 (7), and two novel homozygous variants c.293 G>A; p.C98Y and c.1357T>C; p. C453R identified in two affected families (Fig. 3*A* and *SI Appendix*, *Text* and Fig. S1). The affected children carrying C98Y and C453R variants share overlapping phenotypes with previously reported SHDRA cases, including truncus arteriosus (TA), kidney defects and global developmental delays (Fig. 3*B* and *SI Appendix*, Table S1). We utilized HEK293$^{KO:TMEM260}$ cells and introduced disease variants by site-directed KI (Fig. 3*C*). Western blot analyses indicated that all *TMEM260* variants expressed but were unstable in comparison to the wild-type protein (Fig. 3*D*). Furthermore, KI of these variants revealed markedly reduced ability to rescue and induce O-Man glycosylation on extracellular IPT domains in HEK293$^{KO:TMEM260}$ cells (Fig. 3*E*), verifying that the glycosylation function of TMEM260 is impaired. Interestingly, the *TMEM260* variants from the two newly identified families presenting milder phenotypes (*SI Appendix*, Table S1) and carrying homozygous C98Y or C453R substitutions (*SI Appendix*, Fig. S1 and Table S1), appeared to exhibit some degree of rescue of enzyme function, as evidenced by the differential O-Man glycoproteomic analysis (Fig. 3*E*).

***TMEM260* KO Leads to Receptor Maturation Defects and Abnormal Epithelial Morphogenesis.** We next investigated the endogenous cMET, RON, and Plexin-B2 receptors in human ovarian cancer BG1$^{KO:TMEM260}$ cells by Western blot analysis and observed that maturation of the cMET receptor was not influenced by *TMEM260* KO (Fig. 4). However, proteolytic maturation of both RON and Plexin-B2 was partly affected, with accumulation of the pro-forms in total cell lysates (Fig. 4*A*). Immunofluorescence cytology revealed that Plexin-B2 accumulated in ER with marked reduction in cell surface expression in BG1$^{KO:TMEM260}$ cells

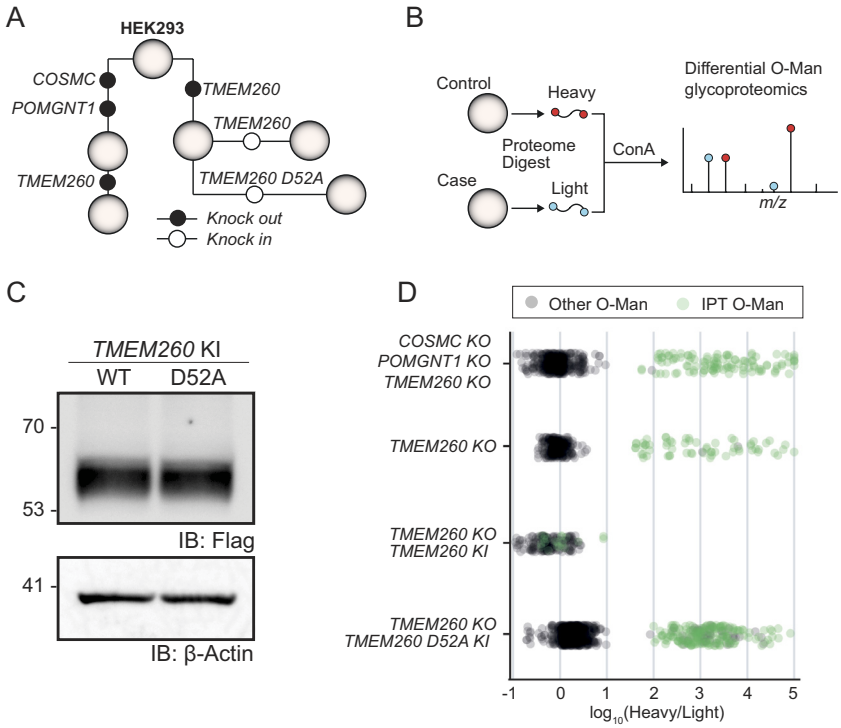

Fig. 2. *TMEM260* knockout selectively abolishes O-Man glycosylation of IPT domains. (*A*) Ancestry of the glycoengineered HEK293 cell panel (gray circles) with knockout (black circle) or site-directed knock-in (hollow circle) of individual genes. (*B*) Strategy for differential O-Man glycoproteomic analysis by mass spectrometry. (*C*) Western-blot analysis of cells stably expressing TMEM260-3×FLAG wild-type or D52A variants. (*D*) Differential O-Man glycoproteomic analysis of HEK293 cell lines with knock-out (KO) and/or knock-in (KI) of TMEM260. Scatter plots show log10 fold change (>1 represents loss of O-mannosylation) of glycopeptide abundances originating from IPT-domains (green dots) or other proteins (e.g., dystroglycan and cadherins).

(Fig. 4*B*). Flow cytometry analysis further confirmed that cell surface expression of cMET was unaffected by loss of TMEM260 O-mannosylation, while cell surface expression of RON and Plexin-B2 receptors were markedly reduced in BG1$^{KO:TMEM260}$ cells (Fig. 4*C*).

Plexin receptors are important for controlled cell division and normal growth in epithelial cells (42, 43). Considering the kidney anomalies found in patients with *TMEM260* deficiencies (7), we turned to a three-dimensional (3D) spheroid model using mouse inner medullary duct epithelial cells (mIMCD-3) (44) and introduced KO of *Tmem260* (*SI Appendix*, Tables S2 and S3). Differential glycoproteomic analyses of mIMCD-3$^{KO:Tmem260}$ cells confirmed selective loss of O-Man glycosylation in IPT domains of cMET and plexin A1, B1, B2, and D1 receptors (Dataset S1). Using two independent clones each of mIMCD-3^{WT} and mIMCD-3$^{KO:Tmem260}$ cells, we found that mIMCD-3^{WT} produced normal spheroids with properly formed lumina and cellular junctions based on apical ZO-1 expression and adherence junctions visualization by E-cadherin immunofluorescence staining, while mIMCD-3$^{KO:Tmem260}$ cells produced spheroids with profound growth and architectural defects (Fig. 5). The mIMCD-3^{WT} cell clones formed an average of 76% and 70% normal cysts, whereas only 20% and 11% of the mIMCD-3$^{KO:Tmem260}$ clones formed normal cysts (Fig. 5*B*). The mIMCD-3$^{KO:Tmem260}$ spheroids (average area of 2.7 mm^2 and 2.9 mm^2) were notably larger in size compared to mIMCD-3^{WT} spheroids, which had an average area of 1.0 mm^2 (Fig. 5*C*), and we further noted that mIMCD-3$^{KO:Tmem260}$ spheroids showed increased number of nuclei per cyst, with an average 46 and 38 nuclei vs. 10 and 13 nuclei for mIMCD-3^{WT} (Fig. 5*D*). These findings indicate that TMEM260-directed O-mannosylation of IPT domains is critical for receptor functions and normal epithelial morphogenesis.

Discussion

Our study elucidated the function of the *TMEM260* gene underlying the SHDRA syndrome and uncovered the genetic and biosynthetic basis for a third distinct type of protein O-mannosylation in higher eukaryotes. We identified TMEM260 as a single O-mannosyltransferase specifically serving IPT domains in cMET, RON and plexin receptors without obvious potential redundancy from paralogs. TMEM260 shares the GT-C fold and overall structure with the POMT and TMTC enzyme families without significant sequence similarities, and the three classes of O-mannosyltransferases serve highly distinct classes of protein clients. Identification of TMEM260 as a glycosyltransferase also establishes SHDRA as a new member of the CDGs (1).

The *TMEM260* gene is conserved in metazoans with distant homologs in bacteria, and the TMEM260-directed O-mannosylation pathway expands the known types of distinct protein glycosylation pathways in mammals to a total of 14 (2, 4). Protein O-mannosylation was originally considered restricted to yeast with a family of seven PMTs that collectively serve a wide set of protein clients (8). A detailed view of the yeast O-glycoproteome revealed that O-Man glycans are widely distributed on many different classes of proteins and positions (45), which much resemble how higher eukaryotes decorate proteins with GalNAc-type O-glycans (2). Interestingly, the two POMT1/2 orthologs of the yeast PMTs appear to serve a quite restricted set of clients, including α-DG and KIAA1549, where O-Man glycosites are positioned in dense mucin-like regions (4, 11, 17, 18). Since these substrate regions are largely unstructured, it is yet unclear how the POMTs drive such high protein client selectivity, but studies have suggested that upstream protein regions may serve as recognition of substrates (46). In contrast, the TMEM260 as well as TMTC1-4 have evolved clear protein domain fold-directed

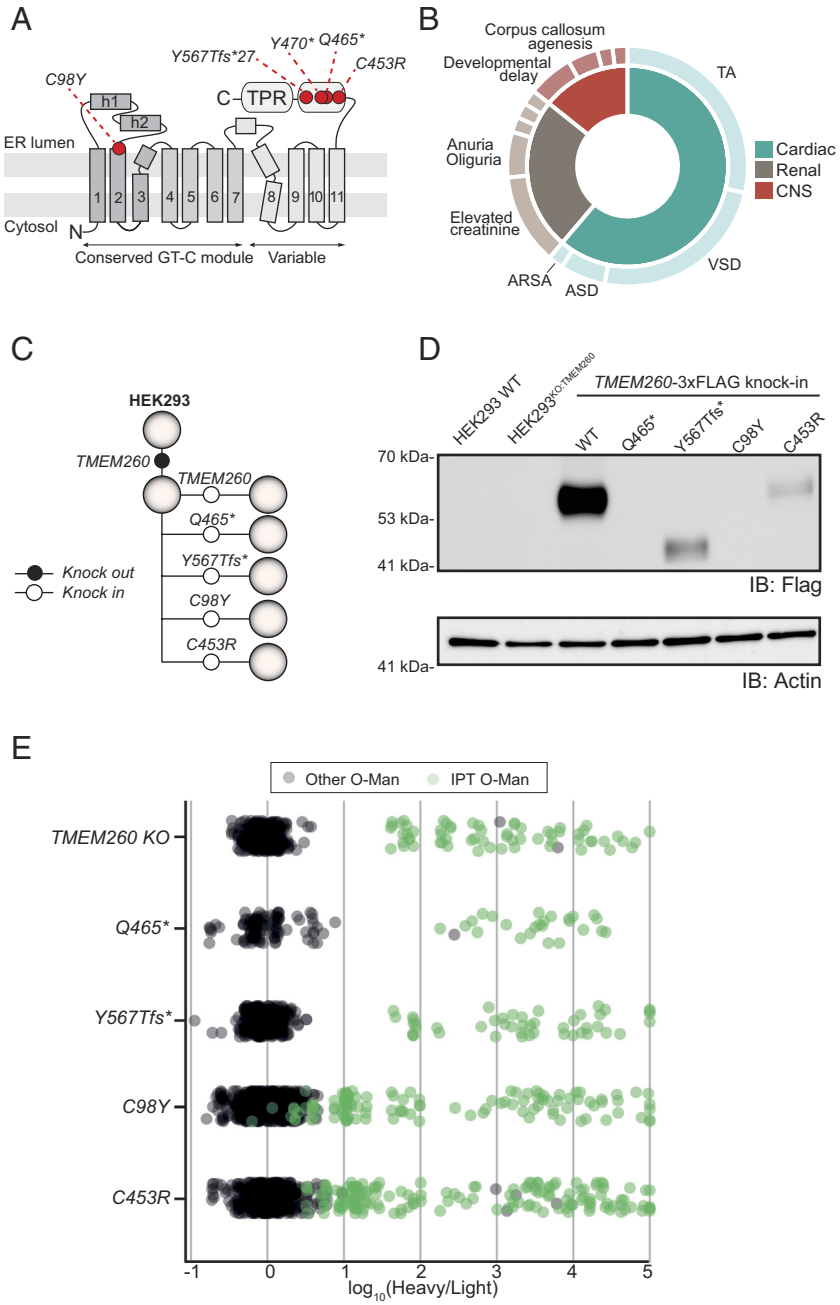

Fig. 3. Loss of function in clinical *TMEM260* variants. (*A*) TMEM260 topology with protein coordinates of clinical mutants indicated as red circles. (*B*) Phenotypic landscape of the SHDRA syndrome. The outer circles represent number of reported cases for truncus arteriosus (TA, n = 13), ventricular septal defect (VSD, n = 13), atrial septal defect (ASD, n = 3), aberrant right subclavian artery (ARSA, n = 1), elevated creatinine (n = 6), anuria/oliguria (n = 3), developmental delay (n = 3) and corpus callosum agenesis (n = 2). (*C*) HEK293 cell panel with knock-in of WT or clinical TMEM260 variants (*D*) Western blot analysis of HEK293^{WT}, HEK293$^{KO:TMEM260}$ and HEK293$^{KO:TMEM260}$ cells stably expressing 3×FLAG-tagged *TMEM260* WT or mutant genes. (*E*) Differential O-Man glycoproteomic analysis of HEK293 cell lines in *C*. Scatter plots show log10 fold change (>1 represents loss of O-mannosylation) of glycopeptide abundances originating from IPT-domains (green dots) or other proteins (e.g., dystroglycan and cadherins).

acceptor substrate specificities to serve highly distinct classes of proteins and biological functions (4, 11). Many other types of protein glycosylation, including O-glucose, O-fucose, O-GlcNAc, and C-Man, are directed by isoenzymes having similar selectivity for specific protein domains (2, 47). The same is clearly not the case for N-glycosylation and the GalNAc-type O-glycosylation that are widely found on proteins and different in different positions and protein folds (2).

Our analysis of disease-causing *TMEM260* mutations clearly confirmed that loss of O-mannosylation underlies the complex phenotypic traits observed in the SHDRA syndrome (6). Moreover, previous studies in zebrafish shows that *tmem260* is required for development in early metazoans (7). Biallelic deleterious nonsense/frameshift mutations in *TMEM260* often lead to early childhood deaths, and patients that survive the first few years of life display neurological phenotypes with global developmental delays (6). We presented two new patients carrying homozygous missense mutations (C98Y and C453R) that are not predicted to affect the catalytic function, but rather appear to influence the stability of TMEM260 (Fig. 3*D*). These mutant enzymes induced partial rescue of O-mannosylation of IPT-domains in our KO cell model (Fig. 3*E*), which may explain the milder phenotype observed in the two affected individuals. Both were diagnosed with TA at birth and have now survived

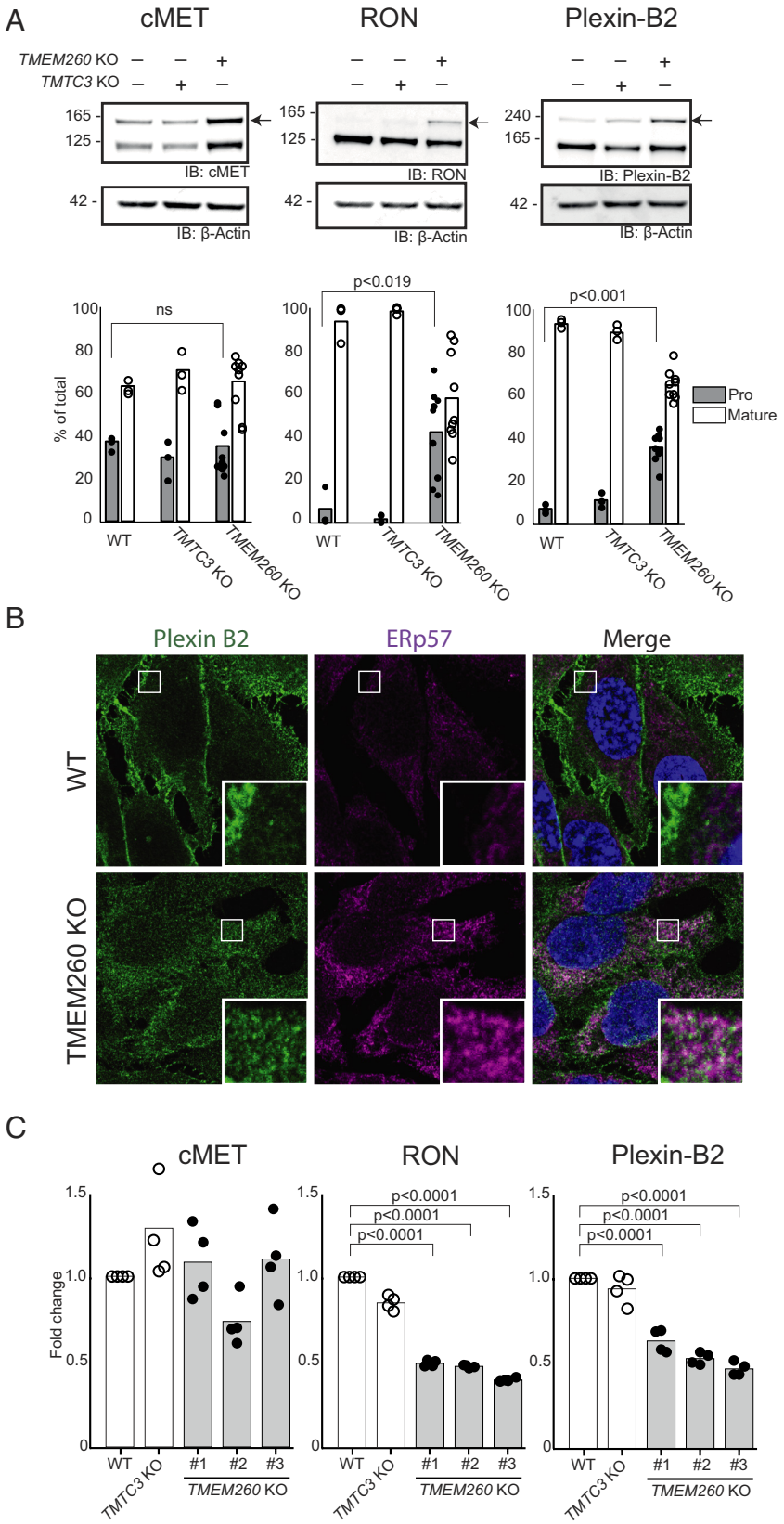

Fig. 4. *TMEM260* KO leads to receptor maturation defects. (*A*) Western blot analysis of total cell lysates of BG1WT and BG1$^{KO:TMEM260}$ cells showing accumulation of larger pro-forms (arrow) of RON and plexin-B2, but not cMET, in *TMEM260* KO cells. Bar graphs show average values for quantification by densitometric analysis of pro- and mature forms over the total intensity (pro-form + mature). The analysis was performed in triplicates for BG1^{WT}, BG1$^{KO:TMTC3}$ (control) and three clones of BG1$^{KO:TMEM260}$. (*B*) Immunofluorescence analysis of BG1^{WT} and BG1$^{KO:TMEM260}$ cells demonstrates retention of plexin-B2 in ER. (*C*) Flow cytometry analysis and quantification of cell-surface expression of cMET, RON and plexin-B2 receptors in BG1^{WT}, BG1$^{KO:TMTC3}$ (control) and BG1$^{KO:TMEM260}$ cells (KO clones #1, #2 and #3), showing reduced cell surface expression of RON and plexin-B2. Statistical analyses were performed by one-way ANOVA, Tukey test.

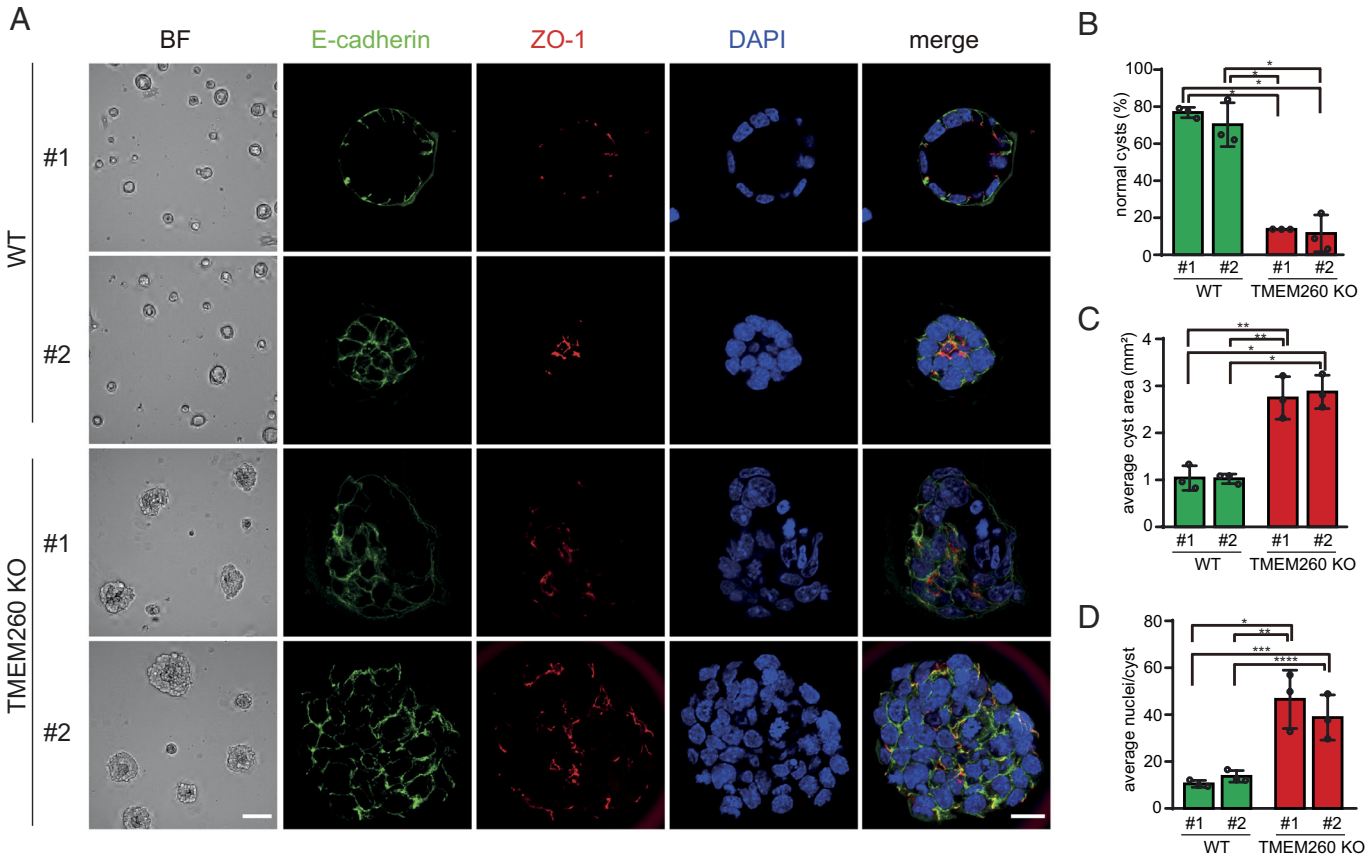

Fig. 5. Loss of *Tmem260* impairs mIMCD-3 spheroid formation. (*A*) Brightfield images ("BF"; scale bar, 100 µm) of mIMCD-3^{WT} (clones #1 and #2) and mIMCD-3$^{KO:Tmem260}$ cells (clones #1 and #2) cultured in matrigel for 3 d. Representative confocal images of anti-E-cadherin (green) and anti-ZO-1 (red) immunostaining are shown (scale bar, 15 µm.) Blue: DAPI. (*B*) Quantification of the percentage of normal cysts based on E-cadherin and ZO-1 immunostaining (n = 3 independent experiments); asterisk (*) indicates $P < 0.0001$. (*C*) Quantification of cyst size based on E-cadherin and ZO-1 immunostaining (n = 3 independent experiments); $^{**}P = 0.0008$ for WT #1 vs. KO #1, $^{*}P = 0.0005$ for WT #1 vs. KO #2, $^{**}P = 0.0008$ for WT #2 vs. KO #1, $^{*}P = 0.0005$ for WT #2 vs. KO #2. (*D*) Quantification of cell numbers per cyst based on DAPI staining (n = 3 independent experiments); $^{*}P = 0.0025$ for WT #1 vs. KO #1, $^{***}P = 0.0106$ for WT #1 vs. KO #2, $^{**}P = 0.0044$ for WT #2 vs. KO #1 or 2, $^{****}P = 0.0206$ for WT #2 vs. KO #2. Statistical analysis was performed by one-way ANOVA, Tukey test.

past the age of 7. They display varying degrees of cognitive impairment with one (C98Y) being nonverbal with autism and the other (C453R) capable of reading/writing and managing mainstream schooling. Interestingly, the rare truncus arteriosus heart defect consistently observed in individuals with bi-allelic *TMEM260* mutations, is also a prominent phenotype in *plexinD1*$^{-/-}$ mice (48) suggesting that O-mannosylation is critical for Plexin-D1 function and related to the heart malformations observed in SHDRA (6).

Glycosylation serves wide roles in folding, transport, and fine-tuning of protein functions (2), and most types of protein glycosylation initiated in the ER affect protein folding and/or stability and transport from ER (49–52). The O-mannosylation initiated in ER by POMTs and TMTCs have so far not been demonstrated to affect folding and transport of client proteins (11, 18). O-mannosylation of α-DG is clearly critical for subsequent building of the matriglycan chain that mediates laminin binding essential for the dystrophin glycoprotein complex (53), but our knowledge of molecular functions of the TMTC and TMEM260 directed types of O-mannosylation is still highly limited and so far these only involve single mannose glycans that are not elongated or modified. Here, we did find that loss of TMEM260-directed O-mannosylation impaired maturation and ER exit of select receptors (Plexin-B2 and RON) (Fig. 4). These observations are reminiscent of the secretion defects and reduced cell-surface expression of receptors that undergo O-Glc and O-Fuc glycosylation by POGLUT1/2 and POFUT1/2, respectively (50, 54). Our use of a 3D spheroid model further support functional roles for O-mannosylation of plexins (and cMET) in epithelial morphogenesis (Fig. 5) but further studies are clearly needed to understand how loss of these single O-Man glycans on specific protein domains have so wide biological effects. The EC domains (55) served by TMTCs and the IPT domains are characterized by varying numbers of antiparallel β-strands assembled into a β-sandwich frame (56, 57). While EC-domains are O-mannosylated by TMTCs on B- and G-strands (11), only the B-strands of IPT domains are O-mannosylated by TMEM260, which may indicate a common role for O-Man in guidance of cadherin and plexin *cis*-interactions at the cell surface.

In conclusion, we provide evidence that *TMEM260* encodes a novel protein O-mannosyltransferase dedicated to IPT domains in select receptor proteins, which serves critical functions during development.

Materials and Methods

Cell Culture. BG1 cells were cultured in RPMI 1640 medium (Sigma) supplemented with 10% Fetal Bovine Serum (FBS) (Gibco) and 1% GlutaMAX (Gibco). HEK293 cells were cultured in DMEM medium (Gibco) supplemented with 10% FBS (Gibco) and 1% GlutaMAX (Gibco). mIMCD-3 cells (25) were cultured in DMEM/F12 medium (Gibco) supplemented with 10% FBS (Gibco) and 1% GlutaMAX (Gibco).

Gene KO/KI Engineering. CRISPR/Cas9 targeted gene KO TMEM260 cell lines were generated as previously reported (11). Briefly, cells were seeded in 6-well plates, transfected the following day with 1.5 μg of PBKS-Cas9-2A-eGFP plasmid (Addgene #68371) and 1 μg gRNA plasmid using Lipofectamine 3000. eGFP positive cells were fluorescence-activated cell sorting (FACS)-enriched 24 h after transfection and single-cell sorted after 1 wk. KO clones were identified by Indel Detection by Amplicon Analysis (11) and validated by sanger sequencing (*SI Appendix*, Tables S2–S4). Site-directed KI of human TMEM260 full coding cDNA into the human AAVS1 safe harbor site was performed using a modified ObLiGaRe gene KI strategy as previously published (58). The donor plasmid pAAVS1 Insulator ObLiGaRe/EPB71 was designed and synthesized by Genewiz, USA (Addgene #90018), and contains CMV-gene of interest-polyA. The full-length TMEM260-3×FLAG WT sequence of donor plasmid was commercially synthesized and cloned in the donor plasmid (Genewiz, USA), and mutations were introduced by site-directed plasmid mutagenesis. Mutations Q465* and Y567Tfs*27 were generated using InFusion DNA polymerase (TaKaRa) and C98Y and C453R using KOD DNA polymerase (Sigma-Aldrich), followed by DpnI (NEB) digestion of donor plasmid and transformation in Stellar competent cells (TaKaRa). Plasmids encoding TMEM260(Q465*)-3×FLAG and TMEM260(Y567Tfs*27)-3×FLAG were generated from the donor constructs using primers in *SI Appendix*, Table S4. All plasmids were confirmed by Sanger Sequencing and a total of seven TMEM260 variant constructs were used for stable cell lines generation. HEK293 TMEM260 KO cells were used as parental strain to generate TMEM260 variant KI cell lines. In brief, 3 μg of donor plasmid and 1.5 μg of each AAVS1 CompoZr Zinc-finger nuclease (ZFN) plasmids (Sigma) encoding ZFN1/2-2A-GFP/E2-Crimson (58) were co-transfected in TMEM260 KO cells using Lipofectamine 3000 (Thermo) according to the manufacturer's protocol. One day after transfection, cells expressing both GFP and E2-Crimson were enriched by FACS (Sony Cell Sorter SH800S), and after 1 wk the bulk populations were single-cell sorted in 96-well plates. Correct stable genomic integration was confirmed using junction PCR of A) the region between the 5′ of AAVS1 genomic locus upstream of the ZFNs cutting site and the 3′ end of the donor construct B) the region between the 5′ end of the donor construct and the 3′ of AAVS1 genomic locus downstream of the ZFNs cutting site.

Dimethyl Labeling of Total Cell Digests for Differential Glycoproteomics. Sample preparation was performed as previously described (11) with minor modifications. Approximately 0.5 mL packed cell pellets were lysed in 1 mL 0.1% RapiGest SF Surfactant (Waters) in 50 mM ammonium bicarbonate by incubation on ice and probe sonication. Extracts were cleared by centrifugation (1,000 g, 10 min), reduced (10 mM dithiothreitol, 37 °C, 30 min) and alkylated (25 mM iodoacetamide, RT, 30 min) before digestion with 25 μg trypsin at 37 °C, 16 h (Roche). Digests were labeled with stable dimethyl isotopes using light or medium dimethyl labels on C18 Sep-Pak columns (Waters), and mixed (1:1 ratio), digested by PNGase F (Sigma, 16U in 150 μL 100 mM Tris, pH 7.4, 37 °C, 16 h), and subjected to ConA lectin weak affinity chromatography (LWAC).

Diethyl Labeling of Total Cell Digests for Differential Glycoproteomics. HEK293 total cell extracts were prepared using S-Trap midi columns (Protifi) with minor modifications to protocol from vendor. Briefly, 0.2 mL packed cells were lysed by probe sonication in 500 μL 5% Sodium dodecyl sulfate (SDS), 100 mM ammonium bicarbonate, cleared by centrifugation (13,000 g, 10 min), reduced (20 mM Dithiothreitol (DTT), 80 °C, 10 min), and alkylated (100 mM iodoacetamide, 30 min, room temperature (RT)). Phosphoric acid was added [final 1.2% (v/v)] and mixed with 3.3 mL 100 mM ammonium bicarbonate in 90% methanol before applied to a S-Trap column. Trypsin (25 μg in 350 μL 100 mM ammonium bicarbonate) was gently applied (37 °C, 18 h), and tryptic peptides eluted by centrifugation [4,000 g, 1 min including a second 50% acetonitrile (ACN), 0.2% formic acid (FA) elution]. Eluates were evaporated, desalted (Sep-Pak C18 100 mg), Speedvac dried, and labeled with stable diethyl isotopes in light (acetaldehyde) or heavy channels (13CH313CHO, Cambridge Isotope Laboratories), as previously described (59). Samples were mixed (1:1 ratio), digested with PNGase F, and subjected to ConA LWAC.

TMT Labeling of mIMCD-3 Total Cell Digests for Differential Glycoproteomics. Proteins were extracted and digested with trypsin in 0.1% RapiGest, 50 mM ammonium bicarbonate as described above. Digest were desalted (Sep-Pak C18), quantified (Nanodrop 205 nm), and 500 μg peptides (each channel) reconstituted (50 mM 4-(2-hydroxyethyl)-1-piperazineethanesulfonic acid (HEPES), pH 8.0), and labeled with 800 μg tandem mass tags (6-plex TMT kit, Thermo). miMCD-3 WT clone #1 and clone #2 were labeled with TMT-126 and TMT-127, respectively. miMCD-3 Tmem260 KO clone #1 was labeled with TMT-128 and TMT-129. miMCD-3 Tmem260 KO clone #2 was labeled with TMT-130 and TMT-131. Labeling efficiency and mixing was evaluated by mass spectrometry. The final 6-plex–labeled tryptic peptide mixture (3 mg) was digested with PNGase F as described above and subjected to ConA LWAC.

ConA LWAC. Digests diluted to 1.5 to 2 mL (25 mM Tris, pH 7.4, 300 mM NaCl, 0.5 mM $MgCl_2$, 0.5 mM $MnCl_2$) were loaded onto a ConA-agarose column (3 m, 100 μL/min) (Vector Laboratories), washed until UV 210 nm absorbance was <5 mAU in same buffer, and eluted with 0.5 M methyl-α-D-mannopyranoside. Fractions were desalted by in-house packed Stage tips (Empore disk-C18, 3M).

Mass Spectrometry. Mass spectrometric analysis of O-Man glycopeptides was carried out as previously described (11). Briefly, desalted samples were individually injected using a EASY-nLC 1000 system (Thermo Fisher Scientific) interfaced via a nanoSpray Flex ion source to an Fusion Tribrid or Fusion Tribrid Lumos mass spectrometer (Thermo Fisher Scientific). The EASY-nLC 1000 was operated using a single analytical column setup (PicoFrit Emitters, 75 μm inner diameter; New Objectives, Woburn, MA) packed in-house with Reprosil-Pure-AQ C18 phase (1.9-μm particle size; Dr. Maisch) at 200 nL/min with gradient step-wise elution using solvent A (0.1% FA) and solvent B (ACN, 0.1% FA) and 2 to 20% B (95 min), 20 to 80% B (10 min), and 80% B (15 min). Precursor MS1 scan (m/z 355 to 1,700) was acquired in the Orbitrap at a resolution setting of 120,000, followed by Orbitrap Higher-energy dissociation (HCD)-MS/MS and electron-transfer/collision-induced dissociation (ETciD)-MS/MS of multiply charged precursors (z = 2 to 6) in the MS1 spectrum; a minimum MS1 signal threshold of 10,000 to 50,000 ions was used for triggering data-dependent fragmentation events; MS2 spectra were acquired at a resolution of 60,000 (HCD and EtciD). For bottom-up analyses of in-gel digests, gradient elution was achieved using 2 to 25% (65 min), 25 to 80% B (10 min), and 80% B (15 min).

Data analyses was carried out using Proteome Discoverer 1.4 software (Thermo Fisher Scientific). Data files (.raw) were processed using the Sequest HT or MS Amanda nodes and searched against the canonical human proteome downloaded (January 2013) from the UniProtKB database (http://www.uniprot.org/). Precursor mass tolerance was set to 10 ppm (Sequest HT) or 5 ppm (MS Amanda) and fragment ion mass tolerance to 0.02 Da. Up to 2 missed trypsin (full- and semi-specific) cleavages were allowed. Carbamidomethylation (cysteine: 57.02146 Da), dimethyl (light: 28.0313 Da, medium: 32.0564 Da), diethyl (light: 56.0626 Da, heavy: 60.07602 Da) and TMT (229.1629 Da) modifications of peptide N-termini and lysines set as fixed modifications. Oxidation (methionine: 15.9949 Da) was set as variable modification. In addition, Hex (162.0528 Da) was set as variable modification for serine and threonine residues. Peptide confidence levels were calculated using the Target Decoy PSM Validator node and results were filtered for high-confidence ($P < 0.01$) identifications only. All spectral matches were inspected manually for validation. Open search was performed via the Fragpipe (v17.1) user interface with MS fragger (v3.4) installed (40). The "glyco-O-open-hybrid" method was used; 162.0528 Da and 324.1056 Da masses were included in the Mass Offsets and Y ion masses lists (MS Fragger). The mass spectrometry proteomics data have been deposited to the ProteomeXchange Consortium via the PRIDE (60) partner repository with the dataset identifier PXD032328. The data may be accessed using the following; username: reviewer_pxd032328@ebi.ac.uk and password: 7pPu1FvF.

M2 Antibody Conjugation to Dynabeads M-270 Epoxy. Mouse M2 antibody (1 mg, F1804-5MG, Sigma-Aldrich) was buffer exchanged (0.1 M sodium phosphate, pH 7.4) using Zebaspin columns (2 mL, Thermo Fischer Scientific), diluted with 500 μL 3M ammonium sulfate in 0.1 M sodium phosphate (pH 7.4), mixed with 50 mg of pre-washed Dynabeads M-270 epoxy (#14302D, Thermo Fisher Scientific), and incubated with rotation at 30 °C (20 to 24 h). Beads were washed (4 × 2 mL Phosphate buffered saline (PBS), 2 × 2 mL 0.5% Triton X-100 in PBS, 2 × 2 mL PBS), and stored in 10% glycerol, 0.02% NaN_3, in PBS up to 3 mo at 4 °C.

Immunoprecipitation of cMET by the M2 Antibody. Cell pellets (300 μL) were lysed in 600 μL (50 mM HEPES, pH 7.4, 50 mM K-Acetate, 200 mM NaCl, 2 mM $MgCl_2$, 1 mM DTT, 0.1% Tween-20, 0.5% Triton X-100), cleared (21,000 g, 10 min, 4 °C), mixed with 60 μL M2-Dynabeads slurry, and incubated with rotation at 4 °C, 45 min. Beads were washed with 3 × 12 mL (50 mM HEPES, pH 7.4, 50 mM K-Acetate, 200 mM NaCl, 2 mM MgCl2, 1 mM DTT, 0.1% Tween-20), and eluted (2×) by incubation in 25 μL with 1 μg/μL FLAG peptide (#F4799,

Sigma-Aldrich) (10 min shaking, RT). The eluate was reduced (10 mM DTT, 37 °C), treated with 1 µL PNGase F (on, 37 °C), diluted in NuPAGE lithium dodecyl-sulfate (LDS) sample buffer, heated (72 °C, 10 min), and separated on a 4 to 12% BIS-Tris sodium dodecyl-sulfate polyacrylamide gel electrophoresis (SDS-PAGE) gel in 3-(N-morpholino) propanesulfonic acid (MOPS) running buffer, and stained with Imperial protein stain (#24615, Thermo Fisher Scientific). Bands migrating at as predicted for pro-MET and mature cMETβ were excised, destained by 3 × 200 µL (50% ACN in 100 mM ammonium bicarbonate, 15 min, 37 °C), followed by addition of 100% ACN, 10 min, RT, to dehydrate. Gel pieces were soaked in 50 µL 5% ACN, 100 mM ammonium bicarbonate containing 0.5 µg trypsin (Roche) at 37 °C ON before addition of 25 µL 100% ACN, 0.1% FA. Extraction was repeated with 2 × 50 µL 50% ACN, and peptides dried (speedvac) and labeled by diethyl stable isotope. Samples immunoprecipitated from HEK293WT were labeled with heavy diethyl (13CH313CHO), while samples from HEK293SC/KO:TMEM260 were labeled with light diethyl (CH3CHO) reagents. Samples were stage-tipped, mixed in equal amounts and subjected to liquid chromatography (LC)-MS/MS.

Treatment with α1-2,3,6-mannosidase (Jack bean, New England Biolab) was performed on immunoprecipitated cMET from HEK293WT cells. In-gel trypsin digest of bands corresponding to cMETβ were split in two and diethyl labeled with heavy diethyl isotopes (mock treatment) and light diethyl isotopes (mannosidase treated). The samples were combined, stage-tipped, and subjected to LC-MS/MS.

Western Blotting. Cells were lysed on ice in buffer (50 mM HEPES pH 7.4, 150mM NaCl, 1% Triton X-100) with 1× complete™ Protease Inhibitor Cocktail (Merck) for 10 min. Lysates were cleared by centrifugation (10 min, 4 °C) and protein amounts were adjusted after BCA assay (#23225, Thermo Scientific), and equal extracts separated on a Bis-Tris 4 to 12% 10-well Mini Protein Gel (Invitrogen) using MOPS or 2-(N-morpholino)ethanesulfonic acid (MES) running buffers. Transfer was performed for 11 min at 20 V to a nitrocellulose membrane using iBlot™ 2 Gel Transfer Device (Thermo Fisher Scientific). Membranes were blocked in a 5% solution of Skim Milk in Tris Buffered Saline with Tween (TBS-T) buffer for 2 h or 30 min. Antibodies used for blotting were diluted according to *SI Appendix*, Table S5. For all blots, primary antibodies were incubated overnight at 4 °C while secondary antibodies were incubated for 1 h at RT with gentle agitation. Blots were developed using SuperSignal™ West Pico PLUS Chemiluminescent Substrate (Thermo Scientific) and imaged by ImageQuant™ LAS 4000 (GE Healthcare). 1 × ReBlot Plus Strong Antibody Stripping Solution (#2504, Merck Millipore) was used for stripping before β-Actin reprobing of membranes. Densitometry analysis was performed using the Gel Analyser function in ImageJ and expressed by quantifying pro- and mature form intensities over the total intensity (pro-form + mature). Statistical analysis was performed by one-way ANOVA, Tukey test.

Immunocytology. BG1 WT and TMEM260 KO cells were grown to 80% confluence, on 10 mm-diameter cover slides, in 24 well plates. The cells were washed once in PBS and fixed with 4% paraformaldehyde for 10 min at RT and quenched with 100 mM NH4Cl in PBS for 10 min. Cells were permeabilized with 0.05% Saponin in PBS with 2 mg/mL bovine serum albumin for 10 min. Cells were stained with primary antibody diluted in permeabilization buffer for 1 h at RT (*SI Appendix*, Table S5). Cells were washed and incubated for 1 h with fluorophore-conjugated secondary antibodies (*SI Appendix*, Table S5) and 4',6-diamidino-2-phenylindole (DAPI). Coverslips were mounted on Mowiol (Calbiochem). Image acquisition was performed using LSM710 (Carl Zeiss) confocal microscope. BG1 WT cells were transiently transfected with TMEM260-3×FLAG, using jetPRIME (PolyPlus) according to manufacturer's protocol. Cells were cultured on 10 mm-diameter cover slides, in 24 well plates. 50 µL of jetOPTIMUS buffer along with 0.5 µg DNA and 1 µL of jetOPTIMUS reagent were mixed and incubated for 10 min before addition to the cells. Media were changed 6 h after transfection and cells were incubated for 24 h before fixation and staining as described above.

Identification of Two Novel *TMEM260* Disease Variants. Family I: A trio whole-exome sequencing was performed on family I using samples from the affected child and both parents. Using genomic DNA from the proband and parents, the exonic regions and flanking splice junctions of the genome were captured using the IDT xGen Exome Research Panel v1.0 (Integrated DNA Technologies, Coralville, IA). Massively parallel (NextGen) sequencing was done on an Illumina system with 100 bp or greater paired-end reads. Reads were aligned to human genome build GRCh37/UCSC hg19, and analyzed for sequence variants using a custom-developed analysis tool. Additional sequencing technology and variant interpretation protocol has been previously described (61). The general assertion criteria for variant classification are publicly available on the GeneDx ClinVar submission page http://www.ncbi.nlm.nih.gov/clinvar/submitters/26957/). A homozygous variant in TMEM260 (c.293 G>A p C98Y) was identified. No other variants were reported. Additional genetic testing included Array CGH, testing for the FMR1 expanded CGG repeat, were normal.

Family II: Whole-exome sequencing was performed using SureSelect Human All Exon V6 (Agilent Technologies) using DNA samples extracted from peripheral blood from the affected individual, an unaffected sibling and both parents. Libraries were sequenced on an Illumina HiSeq 3000 instrument with 6 samples pooled per lane. Reads were aligned to GRCh37 reference genome using Novoalign (Novocraft Technologies, Selangor, Malaysia). Data analysis was performed assuming a homozygous mutation as the most likely cause of disease. Genome Analysis Toolkit HaplotypeCaller was used for variant calling and Ensembl Variant Effect Predictor for variant annotation. Copy number variation (CNV) analysis of WES data was performed using the Exome Depth program in the affected individual. A homozygous TMEM260 variant; 14:57088379T>C, p.C453R, was identified in the affected child and was heterozygous in both parents. In silico tools were supportive of pathogenicity and the CADD score was 25.7. The variant was rare in the Gnomad database (2 of 249,420 alleles, no homozygotes). Two other rare homozygous variants were recognized in the affected individual (in SULT4A1 and C2Orf88), neither of which could be linked to the phenotype. Segregation of the variant identified in TMEM260 was confirmed using conventional Sanger sequencing as homozygous in the affected individual, and heterozygous in both parents and an unaffected sibling.

Data, Materials, and Software Availability. The mass spectrometry proteomics data have been deposited in ProteomeXchange Consortium via the PRIDE (60) partner repository with the dataset identifier PXD032328.

ACKNOWLEDGMENTS. We thank Francis Jacob (University Hospital Basel) for providing BG1 cells and Maxwell L. Bileschi (Google Research, Cambridge, USA) for discussion and analysis of protein domains. This work was supported by Lundbeck Foundation (I.S.B.L.), China Scholarship Council grant 201908080171 (L.Z.), Sir Jules Thorn Biomedical Award JT/09 (C.A.J.), Medical Research Council (MRC)/National Institute of Health Research (NIHR) Clinical Academic Research Partnership award (CARP) fellowship MR/V037617/1 (V.H.), British Heart Foundation clinical research fellowship FS/13/32/30069 (V.H.), Danish National Research Foundation grant DNRF107 (H.C.), Deutsche Forschungsgemeinschaft grant GRK 2213 (T.W.), Novo Nordisk Foundation grant NNF22OC0076899 (H.J.J), Mizutani Foundation for Glycoscience (A.H.) and VILLUM FONDEN grant 00025438 (A.H.).

Author affiliations: [a]Copenhagen Center for Glycomics, Department of Cellular and Molecular Medicine, University of Copenhagen, 2200 Copenhagen N, Denmark; [b]Faculty of Medicine, Institute of Pharmacology, University of Marburg, 35043 Marburg, Germany; [c]Leeds Institute of Medical Research, University of Leeds, St James' University Hospital, Leeds LS2 9JT, United Kingdom; [d]Yorkshire Regional Genetics Service, Chapel Allerton Hospital, Leeds LS7 4SA, United Kingdom; [e]GeneDx, Gaithersburg, MD 20877; [f]Division of Medical Genetics, Department of Pediatrics, Duke University Medical Center, Durham, NC 27710; and [g]Max-Planck-Institute for Heart and Lung Research, 61231 Bad Nauheim, Germany

Author contributions: I.S.B.L., L.P., H.C., T.W., H.J.J., and A.H. designed research; I.S.B.L., L.P., L.Z., W.T., K.J.M., J.H., C.J., V.H., K.P., C.A.J., S.V.M., A.M.-R., M.M., S.Y.V., and A.H. performed research; I.S.B.L., L.P., L.Z., W.T., K.J.M., J.H., C.J., V.H., K.P., C.A.J., S.V.M., A.M.-R., M.M., L.H., S.Y.V., K.T.S., H.C., T.W., H.J.J., and A.H. analyzed data; and H.C., H.J.J., and A.H. wrote the paper.

Competing interest statement: S.V.M. is an employee of GeneDx, Inc. All other authors declare that they have no competing interest.

1. B. G. Ng, H. H. Freeze, Perspectives on glycosylation and its congenital disorders. *Trends Genet.* **34**, 466–476 (2018).
2. K. T. Schjoldager, Y. Narimatsu, H. J. Joshi, H. Clausen, Global view of human protein glycosylation pathways and functions. *Nat. Rev. Mol. Cell Biol.* **21**, 729–749 (2020).
3. C. M. Dobson, S. J. Hempel, S. H. Stalnaker, R. Stuart, L. Wells, O-Mannosylation and human disease. *Cell Mol. Life Sci.* **70**, 2849–2857 (2013).
4. I. S. B. Larsen, Y. Narimatsu, H. Clausen, H. J. Joshi, A. Halim, Multiple distinct O-Mannosylation pathways in eukaryotes. *Curr. Opin. Struct. Biol.* **56**, 171–178 (2019).

5. A. Buczkowska, E. Swiezewska, D. J. Lefeber, Genetic defects in dolichol metabolism. *J. Inherit. Metab. Dis.* **38**, 157–169 (2015).
6. A. T. Pagnamenta *et al.*, Biallelic TMEM260 variants cause truncus arteriosus, with or without renal defects. *Clin. Genet.* **101**, 127–133 (2022).
7. A. Ta-Shma *et al.*, Mutations in TMEM260 cause a pediatric neurodevelopmental, cardiac, and renal syndrome. *Am. J. Hum. Genet.* **100**, 666–675 (2017).
8. L. Lehle, S. Strahl, W. Tanner, Protein glycosylation, conserved from yeast to man: A model organism helps elucidate congenital human diseases. *Angew. Chem. Int. Ed. Engl.* **45**, 6802–6818 (2006).
9. D. Beltran-Valero de Bernabe *et al.*, Mutations in the O-mannosyltransferase gene POMT1 give rise to the severe neuronal migration disorder Walker-Warburg syndrome. *Am. J. Hum. Genet.* **71**, 1033–1043 (2002).
10. J. van Reeuwijk *et al.*, POMT2 mutations cause alpha-dystroglycan hypoglycosylation and Walker-Warburg syndrome. *J. Med. Genet.* **42**, 907–912 (2005).
11. I. S. B. Larsen *et al.*, Discovery of an O-mannosylation pathway selectively serving cadherins and protocadherins. *Proc. Natl. Acad. Sci. U.S.A.* **114**, 11163–11168 (2017).
12. J. Jerber *et al.*, Biallelic mutations in TMTC3, encoding a transmembrane and TPR-containing protein, lead to cobblestone lissencephaly. *Am. J. Hum. Genet.* **99**, 1181–1189 (2016).
13. S. M. K. Farhan *et al.*, Identification of a novel synaptic protein, TMTC3, involved in periventricular nodular heterotopia with intellectual disability and epilepsy. *Hum. Mol. Genet.* **26**, 4278–4289 (2017).
14. J. Li *et al.*, Deletion of Tmtc4 activates the unfolded protein response and causes postnatal hearing loss. *J. Clin. Invest.* **128**, 5150–5162 (2018).
15. H. Guillen-Ahlers *et al.*, TMTC2 variant associated with sensorineural hearing loss and auditory neuropathy spectrum disorder in a family dyad. *Mol. Genet. Genomic Med.* **6**, 653–659 (2018).
16. T. Yoshida-Moriguchi, K. P. Campbell, Matriglycan: A novel polysaccharide that links dystroglycan to the basement membrane. *Glycobiology* **25**, 702–713 (2015).
17. M. B. Vester-Christensen *et al.*, Mining the O-mannose glycoproteome reveals cadherins as major O-mannosylated glycoproteins. *Proc. Natl. Acad. Sci. U.S.A.* **110**, 21018–21023 (2013).
18. I. S. B. Larsen *et al.*, Mammalian O-mannosylation of cadherins and plexins is independent of protein O-mannosyltransferases 1 and 2. *J. Biol. Chem.* **292**, 11586–11598 (2017).
19. K. W. Moremen, R. S. Haltiwanger, Emerging structural insights into glycosyltransferase-mediated synthesis of glycans. *Nat. Chem. Biol.* **15**, 853–864 (2019).
20. A. Shcherbakova, B. Tiemann, F. F. Buettner, H. Bakker, Distinct C-mannosylation of netrin receptor thrombospondin type 1 repeats by mammalian DPY19L1 and DPY19L3. *Proc. Natl. Acad. Sci. U.S.A.* **114**, 2574–2579 (2017).
21. E. Drula *et al.*, The carbohydrate-active enzyme database: Functions and literature. *Nucleic Acids Res.* **50**, D571–D577 (2022).
22. L. Y. Geer, M. Domrachev, D. J. Lipman, S. H. Bryant, CDART: Protein homology by domain architecture. *Genome Res.* **12**, 1619–1623 (2002).
23. K. Tunyasuvunakool *et al.*, Highly accurate protein structure prediction for the human proteome. *Nature* **596**, 590–596 (2021).
24. J. S. Bloch *et al.*, Structure, sequon recognition and mechanism of tryptophan C-mannosyltransferase. *Nat. Chem. Biol.* **19**, 575–584 (2023), 10.1038/s41589-022-01219-9.
25. J. S. Bloch *et al.*, Structure and mechanism of the ER-based glucosyltransferase ALG6. *Nature* **579**, 443–447 (2020).
26. L. Bai, A. Kovach, Q. You, A. Kenny, H. Li, Structure of the eukaryotic protein O-mannosyltransferase Pmt1-Pmt2 complex. *Nat. Struct. Mol. Biol.* **26**, 704–711 (2019).
27. C. Lizak, S. Gerber, S. Numao, M. Aebi, K. P. Locher, X-ray structure of a bacterial oligosaccharyltransferase. *Nature* **474**, 350–355 (2011).
28. L. Bai, T. Wang, G. Zhao, A. Kovach, H. Li, The atomic structure of a eukaryotic oligosaccharyltransferase complex. *Nature* **555**, 328–333 (2018).
29. R. Wild *et al.*, Structure of the yeast oligosaccharyltransferase complex gives insight into eukaryotic N-glycosylation. *Science* **359**, 545–550 (2018).
30. S. Matsumoto *et al.*, Crystal structures of an archaeal oligosaccharyltransferase provide insights into the catalytic cycle of N-linked protein glycosylation. *Proc. Natl. Acad. Sci. U.S.A.* **110**, 17868–17873 (2013).
31. G. L. Blatch, M. Lassle, The tetratricopeptide repeat: A structural motif mediating protein-protein interactions. *Bioessays* **21**, 932–939 (1999).
32. B. Eisenhaber *et al.*, Conserved sequence motifs in human TMTC1, TMTC2, TMTC3, and TMTC4, new O-mannosyltransferases from the GT-C/PMT clan, are rationalized as ligand binding sites. *Biol. Direct.* **16**, 4 (2021).
33. M. B. Lazarus, Y. Nam, J. Jiang, P. Sliz, S. Walker, Structure of human O-GlcNAc transferase and its complex with a peptide substrate. *Nature* **469**, 564–567 (2011).
34. M. Lommel, A. Schott, T. Jank, V. Hofmann, S. Strahl, A conserved acidic motif is crucial for enzymatic activity of protein O-mannosyltransferases. *J. Biol. Chem.* **286**, 39768–39775 (2011).
35. K. R. Geisinger *et al.*, Characterization of a human ovarian carcinoma cell line with estrogen and progesterone receptors. *Cancer* **63**, 280–288 (1989).
36. M. Gouw *et al.*, The eukaryotic linear motif resource–2018 update. *Nucleic Acids Res.* **46**, D428–D434 (2018).
37. K. Akasaka-Manya, H. Manya, A. Nakajima, M. Kawakita, T. Endo, Physical and functional association of human protein O-mannosyltransferases 1 and 2. *J. Biol. Chem.* **281**, 19339–19345 (2006).
38. J. B. Graham *et al.*, Endoplasmic reticulum transmembrane protein TMTC3 contributes to O-mannosylation of E-cadherin, cellular adherence, and embryonic gastrulation. *Mol. Biol. Cell* **31**, 167–183 (2020).
39. J. C. Sunryd *et al.*, TMTC1 and TMTC2 are novel endoplasmic reticulum tetratricopeptide repeat-containing adapter proteins involved in calcium homeostasis. *J. Biol. Chem.* **289**, 16085–16099 (2014).
40. D. A. Polasky, F. Yu, G. C. Teo, A. I. Nesvizhskii, Fast and comprehensive N- and O-glycoproteomics analysis with MSFragger-Glyco. *Nat. Methods* **17**, 1125–1132 (2020).
41. M. O. Sheikh, S. M. Halmo, L. Wells, Recent advancements in understanding mammalian O-mannosylation. *Glycobiology* **27**, 806–819 (2017).
42. J. Xia *et al.*, Semaphorin-plexin signaling controls mitotic spindle orientation during epithelial morphogenesis and repair. *Dev. Cell* **33**, 299–313 (2015).
43. C. Jiang *et al.*, Mechanochemical control of epidermal stem cell divisions by B-plexins. *Nat. Commun.* **12**, 1308 (2021).
44. R. H. Giles, H. Ajzenberg, P. K. Jackson, 3D spheroid model of mIMCD3 cells for studying ciliopathies and renal epithelial disorders. *Nat. Protoc.* **9**, 2725–2731 (2014).
45. P. Neubert *et al.*, Mapping the O-mannose glycoproteome in Saccharomyces cerevisiae. *Mol. Cell Proteom.* **15**, 1323–1337 (2016).
46. I. Breloy *et al.*, Initiation of mammalian O-mannosylation in vivo is independent of a consensus sequence and controlled by peptide regions within and upstream of the alpha-dystroglycan mucin domain. *J. Biol. Chem.* **283**, 18832–18840 (2008).
47. B. M. Harvey, R. S. Haltiwanger, Regulation of notch function by O-Glycosylation. *Adv. Exp. Med. Biol.* **1066**, 59–78 (2018).
48. A. D. Gitler, M. M. Lu, J. A. Epstein, PlexinD1 and semaphorin signaling are required in endothelial cells for cardiovascular development. *Dev. Cell* **7**, 107–116 (2004).
49. M. Ogawa, T. Okajima, Structure and function of extracellular O-GlcNAc. *Curr. Opin. Struct. Biol.* **56**, 72–77 (2019).
50. B. C. Holdener, R. S. Haltiwanger, Protein O-fucosylation: Structure and function. *Curr. Opin. Struct. Biol.* **56**, 78–86 (2019).
51. A. Helenius, M. Aebi, Roles of N-linked glycans in the endoplasmic reticulum. *Annu. Rev. Biochem.* **73**, 1019–1049 (2004).
52. S. Varshney, P. Stanley, Multiple roles for O-glycans in Notch signalling. *FEBS Lett.* **592**, 3819–3834 (2018).
53. E. Hohenester, Laminin G-like domains: Dystroglycan-specific lectins. *Curr. Opin. Struct. Biol.* **56**, 56–63 (2019).
54. H. Takeuchi *et al.*, Two novel protein O-glucosyltransferases that modify sites distinct from POGLUT1 and affect Notch trafficking and signaling. *Proc. Natl. Acad. Sci. U.S.A.* **115**, E8395–E8402 (2018).
55. O. J. Harrison *et al.*, The extracellular architecture of adherens junctions revealed by crystal structures of type I cadherins. *Structure* **19**, 244–256 (2011).
56. Y. Kong *et al.*, Structural basis for plexin activation and regulation. *Neuron* **91**, 548–560 (2016).
57. E. Uchikawa, Z. Chen, G. Y. Xiao, X. Zhang, X. C. Bai, Structural basis of the activation of c-MET receptor. *Nat. Commun.* **12**, 4074 (2021).
58. R. Pinto *et al.*, Precise integration of inducible transcriptional elements (PrIITE) enables absolute control of gene expression. *Nucleic Acids Res.* **45**, e123 (2017).
59. J. Jung *et al.*, Deuterium-free, three-plexed peptide diethylation for highly accurate quantitative proteomics. *J. Proteome. Res.* **18**, 1078–1087 (2019).
60. Y. Perez-Riverol *et al.*, The PRIDE database resources in 2022: A hub for mass spectrometry-based proteomics evidences. *Nucleic Acids Res.* **50**, D543–D552 (2022).
61. K. Retterer *et al.*, Assessing copy number from exome sequencing and exome array CGH based on CNV spectrum in a large clinical cohort. *Genet. Med.* **17**, 623–629 (2015).